UNCONVENTIONAL ADSORPTION OF ALKANE SUBSTITUTED NAPHTHALENE DIIMIDES ON HIGHLY ORDERED PYROLYTIC GRAPHITE

By

CLARISA MICHELLE CARRIZALES

A thesis submitted in partial fulfillment of
the requirements for the degree of

MASTER OF SCIENCE IN CHEMISTRY

WASHINGTON STATE UNIVERSITY
Department of Chemistry

AUGUST 2009

To the Faculty of Washington State University:

The members of the Committee appointed to examine the thesis of CLARISA MICHELLE CARRIZALES find it satisfactory and recommend that it be accepted.

_____
Kerry W. Hipps, Ph.D.,Chair

_____
Ursula Mazur, Ph.D.

_____
Aurora Clark, Ph.D.

ACKNOWLEDGEMENTS

First and foremost, I would like to thank the Lord, my God for giving me the strength, wisdom, and knowledge to get through. Without Him I am nothing and I couldn't have done this without Him in my life. I surely would have gone crazy.

Secondly, I have to thank my family, most especially my parents, Rachel and Cristobal Carrizales, for their support throughout everything. It is because of them I am where I am. They are the ones who were always there encouraging me to follow my dreams. They taught me the importance of furthering my education, but they also taught me that love and hard work can get you through anything.

Thirdly, I'd like to thank my advisor, K.W. Hipps, for guiding me through this project and putting up with me through my lows and highs. Thank you for your advice and the knowledge you bestowed upon me. It might not seem at times like I was picking it up or paying attention, but I was listening and have learned a lot through it all.

I'd also like to thank all the professors that I have worked with and taken classes from. Thank you for your knowledge and for helping me to understand Chemistry on a deeper level.

Finally, to all my friends, both graduate and undergraduates. Special thanks go out to Leslie Shuhler for all her hard work on the project I ultimately took over from her. Also, thanks go out to Casey Bloomquist for finishing off some of the imaging on this project while I've been busy finishing off this thesis. And finally a special thanks to Krista Nishida for being a great friend and encouraging me through the good times and bad.

UNCONVENTIONAL ADSORPTION OF ALKANE SUBSTITUTED NAPHTHALENE DIIMIDES ON HIGHLY ORDERED PYROLYTIC GRAPHITE

Abstract

by Clarisa Michelle Carrizales, M.S.
Washington State University
August 2009

Chair: Kerry W. Hipps

Scanning Tunneling Microscopy (STM) is reported for N, N'-Dihexyl-1,8:4,5 naphthalenediimide (C_6 NDI), N, N'-Dioctyl-1,8:4,5-naphthalenediimide (C_8 NDI), and N, N'-Didodecane-1,8:4,5-naphthalenediimide (C_{12} NDI) adsorbed on highly ordered pyrolytic graphite (HOPG). All three naphthalenediimides (NDI) formed well ordered monolayers at the interface between the HOPG and different alkylbenzenes. C_8 NDI was also adsorbed from toluene at both the HOPG-air and HOPG-vacuum interface. Planar adsorption of the C_6, the C_8 and C_{12} NDI ring cores on HOPG was observed. All three NDIs were observed to have the same monolayer structure, but in order to fit them to the structure, their alkane arms were at an angle to the NDI ring core which lay flat relative to the surface of the HOPG. Hydrogen bonding, O and N interaction with HOPG, and π-π interactions all appear to play a primary role in the creation of the monolayer structure. The monolayer structure had no dependence on the adsorption method and was stable. Other alkane substituted systems in previous studies which form adsorbate structures on graphite are driven by alkane chain interactions with HOPG and interdigitation. The observed unit cell for C_6 NDI has a= 2.11±0.04 nm, b= 1.75±0.14 nm, and α=

67.02±2.39°. The observed unit cell for C_8 NDI in solution has a= 1.98±0.25 nm, b= 1.73±0.25 nm, and α= 68.00±2.00°. The observed unit cell for C_8 NDI cast films in UHV is a=1.97 ± 0.20 nm, b=1.95 ± 0.20 nm, and α= 66.00 ± 2.00º. The observed unit cell for C_{12} NDI has a=1.95 ± 0.10 nm, b=1.93 ± 0.09 nm, and α=72.60 ± 2.60º. The STM imaging is highly dependent on the bias and appears to be controlled by an unoccupied orbital in the ±2 V bias region. Orbital mediated tunneling spectroscopy (OMTS) was performed on C_8 NDI. The spectra revealed a single electron affinity band near 3.5 eV below the vacuum level.

TABLE OF CONTENTS

LIST OF FIGURES

LIST OF TABLES

Page

CHAPTER 1: INTRODUCTION

Scanning Tunneling Microscopy (STM) has allowed scientists to become intimately familiar with various surfaces. In particular, there have been various studies conducted involving adsorbate structures on graphite (highly oriented pyrolytic graphite or HOPG) surfaces. These studies have included solid-solution and solid-atmosphere interface studies with a recent interest in organic[1-12] and metalorganic[13-19] molecules with alkane substituents. Previous studies of these molecules at the solid-solution interface have shown well-ordered two-dimensional monolayers. The two-dimensional ordering of the monolayers is affected by the number and length of the alkyl chain substituents.[20] This allows for the molecules in the monolayer to pack in a lamellar structure. By increasing or decreasing the lengths and numbers of alkyl chain substituents, control over the position and orientation of the molecules is possible.[20-23] The literature is full of images with sub-molecular resolution of well-ordered two dimensional monolayer structures at the solvent-HOPG interface.

Also of more recent interest, is the effect that different solvents have on solute-surface interactions.[20,24-29] There are four criteria that an organic solvent should meet in order for it to be used for solute-surface interface studies.[24] They must have a low vapor pressure, be electrochemically inert, solubilize the compound of interest, and have a low affinity for adsorption on the substrate. The mixture of the compound and the solvent can lead to various types of monolayers.[24] In one type of monolayer, the different molecules organize into separate domains.[27,30] In another type, the solvent molecules and the compound of interest form a mixed domain where the solvent molecules coadsorb inside the two-dimensional molecular network.[24,31,32] The coadsorption of solvent molecules

depends on the size and shape of the molecules as well as their interaction with the other molecules.[25] The mobility of the molecules, such as their ability to adsorb and desorb at the solute-surface interface, is also affected by the solvent.[25]

In order to reduce the affects the solvent can have on the two-dimensional monolayer structure, there have also been a few STM studies of cast films (monolayers formed from solution then dried) on graphite.[33-35] Well-ordered monolayer structures can still be imaged with molecular resolution in these types of studies. Stable monolayers have also been formed both at the solution-solid interface and in UHV; however, there are few studies where this has been achieved for the same molecule in both environments.[36,37]

Now the question is why are these types of studies important? What if anything do they bring to the table? An understanding of substrate-adsorbate, adsorbate-adsorbate, and adsorbate-solvent interactions is essential to the creation and design of new nanoscale materials.[38-41] These interactions can be manipulated to give desirable properties, and in such a way, are useful in the development of new technologies. However, for these structures to be used to their full potential more than their atomic structures must be understood. For a study of adsorbate structures to be complete, both the molecular structure of the adlayer in both the solid-solution and the solid-air/solid-vacuum interface, as well as the electronic energy levels of the structure must be studied. One way of studying the occupied and unoccupied electronic energy states with the STM is through orbital mediated tunneling spectroscopy (OMTS).[42,43] OMTS allows the locations of the HOMO and LUMO to be determined. This is important because the HOMO and LUMO

of these structures dominate properties such as electrical conductivity, optical absorption, and electron transfer kinetics.

For this particular study, the STM of alkane substituted 1,4,5,8-naphthalenediimides (NDI) is presented (Figure 1).[44] These molecules have been found to be useful due to their tendency to form n-type semiconducting materials.[45] They are a compact, electron deficient class of aromatic compounds capable of self-organization[46] and with a rich potential for interaction on and with the HOPG surface.[44] The NDIs that are presented in this study have been substituted with alkane chains of varying lengths. These alkane chains are thought to play an important role in the creation of a well-ordered adlayer on HOPG.[44] NDIs contain the electronegative species of oxygen and nitrogen which provide it with an electronegative component with at least one electronic state within the OMTS's accessible region.[44] Another effect of these species is that they hydrogen bond and interact with the substrate through induced dipolar interactions.[44] NDIs in the solid-state have exhibited stacking

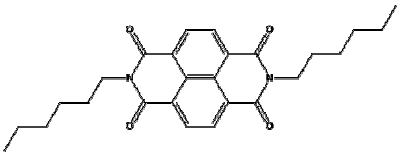

N,N'-Dihexyl-1,8:4,5-naphthalenediimide

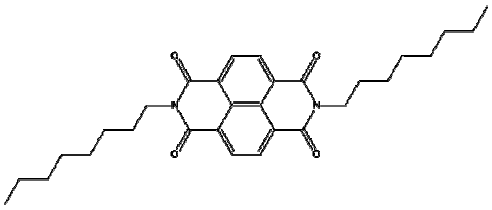

N,N'-Dioctyl-1,8:4,5-naphthalenediimide

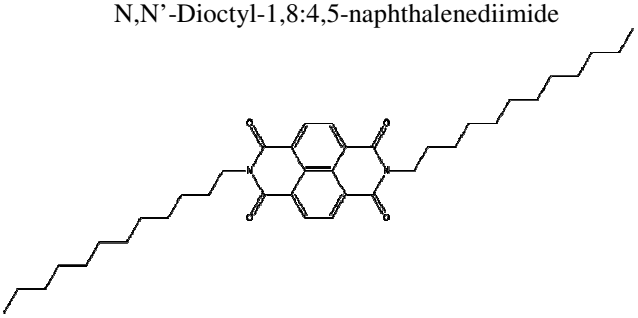

N,N'-Didodecane-1,8:4,5-naphthalenediimide

Figure1: Alkane substituted Naphthalene diimides.

with distances commensurate with π-π stabilization due to its planar aromatic nature.[47] It is these π-π interactions between the large aromatic ring and the HOPG that are believed to influence the surface packing structure. NDIs contain a lipophilic naphthyl core and four polar carbonyl groups that greatly influence their solubility in various solvents.[47] Depending on the imide substituents NDIs are usually soluble in low polarity lipophilic solvents (toluene, DCM, chloroform, etc.) and polar aprotic solvents (acetonitrile, DMF, DMSO, etc.).[47] The solvents in this study were chosen based on this information.

The present study will demonstrate the interaction between the HOPG surface and the NDIs in various solvent and solvent-free situations. It will be seen that the presence or lack of solvent and a change in solvent at the interface will not affect the monolayer structure and therefore it is the interaction between the substrate and the NDIs that dominate the adlayer structure. Also a change in the length of the alkane chain does not affect the monolayer structure. Therefore, this study will show that, contrary to conventional expectations, it is the interaction between the NDI core and the HOPG surface that affects the monolayer structure. UHV and OMTS data will also be presented for N, N'-dioctyl-1,8:4,5-naphthalenediimide.

CHAPTER 2: EXPERIMENTAL SECTION

2.1 TIP PREPARATION

In STM studies, the tip is an essential aspect of the imaging process. Its stability, which is influenced by the size, shape, and the chemical identity of the tip, greatly influences the resolution, shape of the STM scan and the measured electronic structure.[48] In order for a tip to be considered reliable, it must meet three criteria (Figure 2).[49] The first is a blunt macrostructuring of the shank. This allows for higher data rates by minimizing phase hysteresis and allowing a high flexural resonant frequency. The second is an atomic microstructure of the tip. This is key to image resolution as the tunneling current is exponentially dependent on the gap distance (Figure 3).[50] For tunneling through a simple square barrier, $I=cV\exp(-1.02d\sqrt{\Phi})$, where I is the tunneling current, d is the distance in Angstroms, and Φ is the work function in eV. It is necessary to have a single site interacting with the surface because for normal conditions, approximately 90% of the current is carried by the apical atom on the tip.[51] The tip must be well supported and must not have any whiskers. When there are multiple atoms or

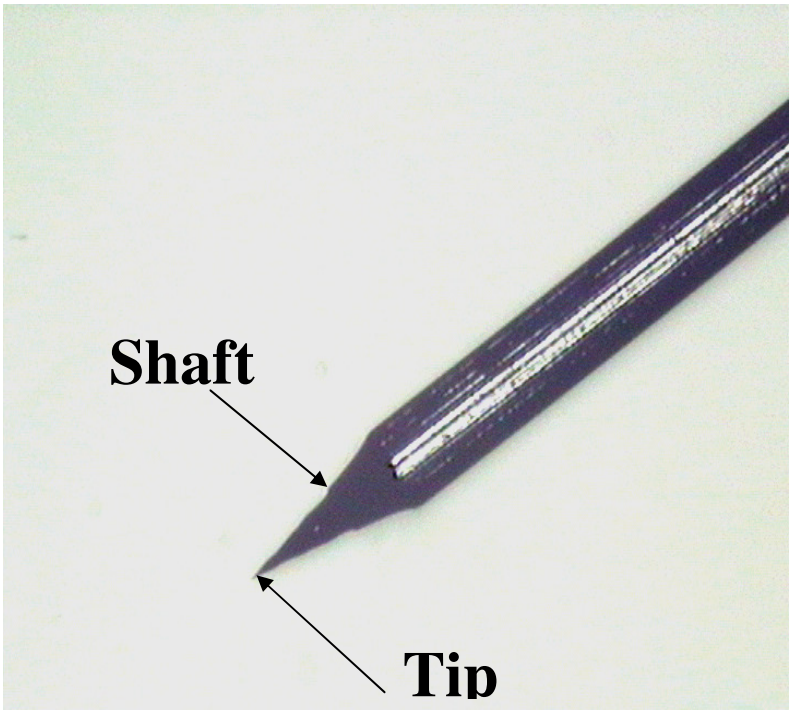

Figure 2: The different parts of a tip.

"tips" on the tip, simultaneous tunneling (double tip imaging or ghost images) will occur. The last criterion is tip purity. It is important when making a tip that there is no series barrier. For example tungsten is known to easily oxidize in air, thereby creating an oxide layer on the tip. This oxide layer's effective resistance can be higher than the desired tunneling gap resistance; therefore, mechanical contact of the tip and the sample would occur before the required tunneling current could be obtained. Also, a metallic tip is preferred over a non-metallic tip as the non-metallic tip may have a rapidly varying density of states and therefore not represent the true electronic structure of the sample surface when taking spectra.

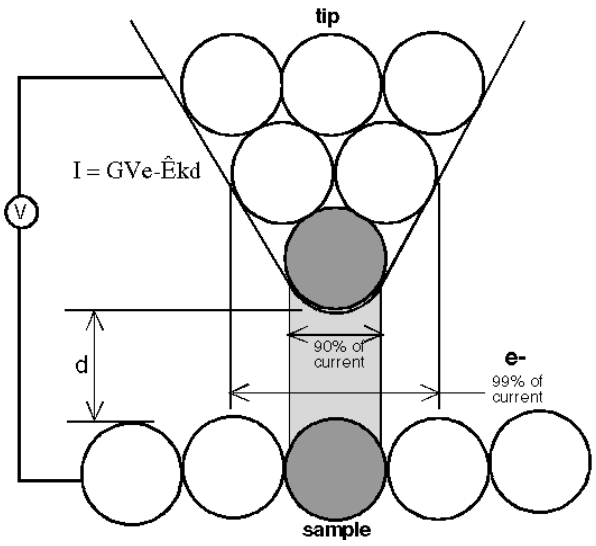

Figure 3: Schematic of tip and sample interaction for STM.[50]

Tips can be made of several different metals. The two metals used in the current study are tungsten (W) and platinum iridium ($Pt_{0.8}Ir_{0.2}$).[48] Tungsten is a stiff metal that produces atomically sharp tips. However, it forms oxide layers on the surface of the tip in the air making it difficult to acquire STM images at ambient conditions. For this reason, tungsten is preferred in UHV systems. Platinum is a soft metal and although it does not produce tips as sharp as tungsten it is preferred over tungsten in solution or in air because it is relatively inert to oxidation. To add stiffness while maintaining inertness, iridium (Ir) is usually added to create a Pt/Ir alloy. PtIr tips are widely employed in atmospheric and electrochemical environments.

A. Tungsten Tip Annealing

There is a need to increase the stability and sharpness of tips used for STM. As stated before, tungsten produces sharper tips than PtIr and according to previous studies in the literature, single crystal tungsten wire can be used to produce atomically sharp tips that are mechanically stable and have a well-defined shape for STM studies.[48,52,53] However, due to cost, the tungsten tips most commonly used are cold-drawn, polycrystalline wire (CDW) tips. Because the atomic scale structure of CDW is uncontrollable, using CDW often leads to tips with multiple protrusions at the apex making them structurally unstable and leading to image artifacts (tunneling occurs through more than one protrusion at once.).[48] Besides causing image artifacts, multiple protrusions can lead to tip instabilities during imaging. It is possible that the protrusion separates itself from the tip during imaging and attaches to the sample surface,[52,54] something that is not seen when using single crystal tungsten. These problems are thought to occur because of the extremely high defect concentrations in the grains of the CDW. To alleviate the problems associated with CDW, M. Greiner and P. Kruse[55] developed a method of annealing the wire prior to the fabrication of the tip to reduce the defect concentration of the CDW, allowing tips to be formed from more pristine crystals.

Annealing is the process by which deformed metals are recrystallized. In order to anneal the wire, it must be heated to a temperature well below its melting point, but high enough that solid state diffusion can occur at a high enough rate.[55] During this process, the wire undergoes changes in its internal structure (Figure 4).[55] First the point defects and dislocation densities in the grains are reduced in a process known as recovery. Then recrystallization occurs. This is the point where new, pristine grains begin to nucleate in highly deformed regions. The grains grow and consume the previously deformed grains. Finally, after recrystallization, grain growth occurs and a few grains further increase in size. Through this process a more crystalline tungsten wire is acquired from which a good tip can be formed through a process known as electrochemical etching.

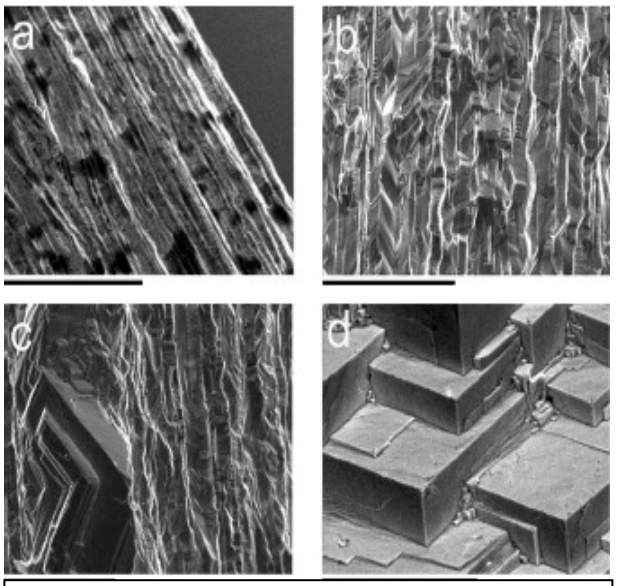

Figure 4: SEM images showing grain structure of (a) unannealed W wire and wires annealed at 6.7 A for (b) 10 s, (c) 1 min, and (d) 30 min. Scale bars are 20 μm[55]

B. Electrochemical Etching

There are many factors that affect the electrochemical etching of a metal wire. The choice of the electrolyte and the voltage depends on the material being etched. In the case of tungsten, sodium hydroxide (NaOH) is used. For PtIr, sodium chloride (NaCl) is used. Since tungsten is much more reactive during the etching process then PtIr, tungsten is etched at a much lower voltage than PtIr. The etch cut-off time, which is the time between the actual drop-off and the switching off of the circuit, affects the sharpness of

the tip.[48,56] The longer the etch cut-off time, the more blunt the resulting tip will be. This is due to the fact that the electrochemical reaction does not stop after drop-off. Therefore, if the applied voltage is not turned off right away, the sharpened end of the tip will continue to be etched away.

The tip's shape is directly influenced by the shape of the meniscus.[48,56] The shorter the meniscus is, the smaller the aspect ratio of the resulting tip. A short aspect ratio limits vibration of the tip in STM. A symmetric meniscus yields a symmetric tip; therefore, any disruption of the meniscus produces undesirable tips for STM. The most common disruption to the meniscus occurs because of the development of hydrogen bubbles. The concentration of the electrolyte affects the etching time and also affects the meniscus.[48,56] A low concentration electrolyte leads to long etching times. These long lengths of time increase the chances of dirt particles and bubbles disturbing the meniscus. At higher concentrations, the reactions are faster. If the concentration is too high the reaction may turn violent, which will cause a quick change in the cross-sectional area of the wire. This will in turn cause the meniscus to drop.

Another factor affecting the etching of a metal wire is the applied voltage, both the type and the amount of voltage.[48,56,57] AC voltage is known to form many gas bubbles around the surface of the wire. This causes etching to occur above the air/electrolyte interface. A protective layer about the lower end of the wire cannot form which causes delocalized electrolytic attack. Because of these effects, AC voltage produces longer tips with a long taper. DC voltage is preferred for electrochemical etching, more specifically at low voltages. The low voltage encourages localized electrolytic action which produces sharp tips with a pronounced concave shape. At high

voltage, the drop-off becomes improbable because the high reaction rate quickly etches the lower part of the wire before the neck can be etched.

The final factor that affects the etching process is the length of the wire that is immersed in the solution.[48,56] If the dipping length is too small, there will be no necking phenomenon. However, if the dipping length is too long, the weight of the part hanging below the necking point may cause a premature drop-off and thereby causing a blunt tip. The trick to producing reliable STM tips is to find a happy medium between all these factors. This study addresses the differences as far as shape and reliability of the tip. STM imaging was done on graphite using both the unannealed and annealed W wire tips and also PtIr tips to determine whether or not the annealing process improved the utility of the W tips for the other experiments in this study.

C. Annealing Experimental Procedure

Annealing was performed using a modified titanium sublimation pump (TSP) cartridge filament source capable of supporting three 0.25 mm diameter, 99.95% tungsten wires (Alfa Aesar) about 10 inches long (Figure 5). The modified fixture was mounted on a high vacuum chamber and an external DC power supply in constant current mode was used to resistively heat the wire. Annealing was accomplished by running 6.7 A of current through each wire (one at a time) in vacuum at a pressure of approximately 10^{-6} torr for 30 minutes per wire.[55]

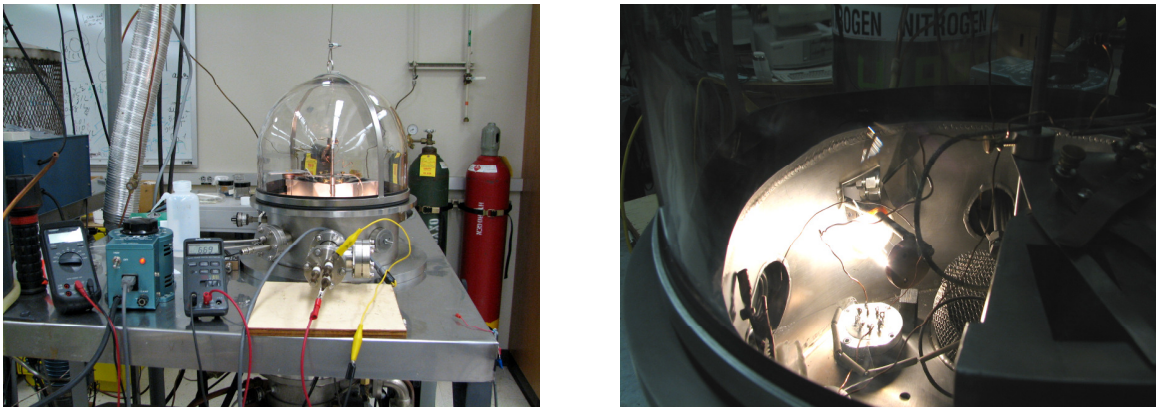

Figure 5: High vacuum setup for Tungsten annealing.

D. Tungsten Electrochemical Etching Procedure

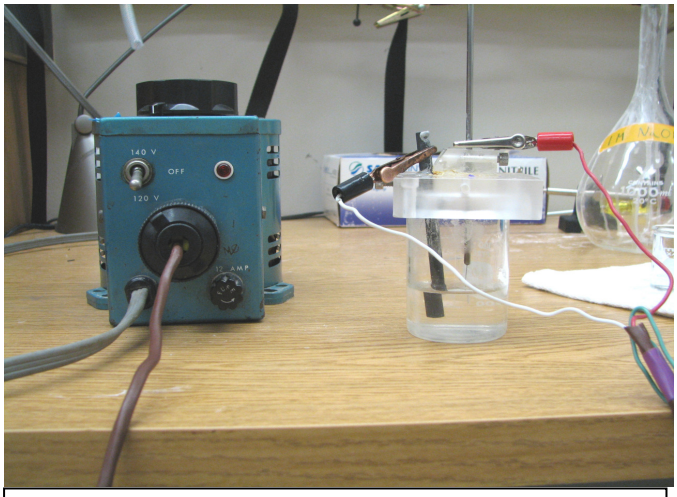

Figure 6: Tungsten Electrochemical Etching Setup.

A 250 mL beaker was filled ¼ of the way with 1 M NaOH (J.T. Baker, NaOH pellets). Three small beakers were filled with millipore (mp) water. Tungsten wire was cut to approximately 20 mm. The wire was placed in the holder (Figure 6) and the height of the pole was adjusted until the whole wire length, but not the holder itself, was immersed in the solution. The wire was pre-etched for 1 to 2 seconds at the desired AC voltage (5V, 7V, 15V, 25V, 30V). The pole height was then adjusted until the tip of the wire just barely touched the surface of the solution. It was then moved down approximately 5 mm. For course etching, the wire was etched at the desired voltage until finished. After course etching, the pole was adjusted until the whole wire length was dipped into the solution and the wire was post-etched at the same

voltage as before for 1 to 2 seconds. Finally, the wire was dipped into three sequential beakers of mp water for 10 seconds in each.

2.2 STM

A. Materials

The naphthalene diimides were prepared by known methods.[58] All organic solvents were used as supplied and are commercially available from either Alfa Aesar (n-hexylbenzene, n-heptylbenzene, and n-octylbenzene) or Aldrich (n-decylbenzene and toluene).

Solutions of C_6 NDI in n-octylbenzene were made at a concentration of $1x10^{-4}$ M. C_6 NDI was brought into solution by sonication for 30 minutes. Solutions of C_8 NDI in n-hexylbenzene, n-octylbenzene, and n-decylbenzene were made at a concentration of $5x10^{-4}$ M, $4x10^{-4}$ M, and $2x10^{-3}$ M respectively. C_8 NDI was brought into all three solutions by heating the solutions to approximately 55°C. A solution of C_8 NDI in toluene was also made for cast films. C_8 NDI was readily soluble in toluene at the mM level. This solution was made at a concentration of $2x10^{-3}$ M. Finally, solutions of C_{12} NDI in a 50/50 solution of toluene and n-octylbenzene were made at a concentration of $3x10^{-4}$ M. C_{12} NDI was brought into solution by sonication.

B. Ambient and Solution STM

A stand alone STM (originally by Digital Instruments, now Veeco) was used using a NanoScope E controller and version 4 of the software. Tips were made with $Pt_{0.8}Ir_{0.2}$ wire of 0.010 mm diameter and W wire of 0.25 mm diameter and etched in 1 M NaCl and 1 M NaOH solutions. Samples in solution were prepared by placing a drop of

the NDI's in the various alkylbenzene solutions on the surface of a piece of freshly cleaved HOPG, grade 2 from SPI supplies. For solution STM imaging, the tip was inserted through the solution layer. Large areas of organized monolayers could be seen as well as grain boundaries and defects in these samples. In the case of cast films, a drop of the NDI solutions in toluene was placed on the surface of freshly cleaved HOPG and was allowed to evaporate under argon. In order to acquire images, currents between 15 to 25 pA and a sample bias ranging from +1.2 and +1.8 V were used. If the bias settings were more negative than 1 V and the current > 100 pA, the image would be lost.

C. UHV STM

The sample used for the UHV studies was a cast film made from the $2x10^{-3}$ M solution of C_8 NDI in toluene. After being dried under argon the sample was inserted into the UHV-STM purchased from RHK and controlled by RHK electronics and software. Once transferred into UHV, the sample was heated to 91°C for 7 minutes to remove excess molecules adsorbed on the surface of the monolayer. The UHV chamber routinely operates at pressures below $1x10^{-10}$ torr. The images collected in UHV were done in constant current mode and calibration was performed based on the known lattice spacing of clean graphite. To obtain high quality spectra and assure the cleanliness of the tips, electrochemically etched, annealed W tips were transferred into an attached vacuum chamber and were argon ion sputtered at 1 kV with a beam current of > 10 μA for 60-120 seconds, then were directly transferred into the main UHV chamber. Using the RHK software with the feedback loop off during current-voltage (IV) scans, IV curves were acquired. Anywhere from 9 to 30 curves were acquired and coadded and produced essentially the same curves. Based on this it is clear that sputtered clean tips provide

excellent reproducibility. The same lattice structure that was observed in both air and solution could also be seen in the images taken with the sputtered W tips in UHV. As in solution experiments, the images were acquired at 15 to 25 pA and +1.2 to +1.8 V. There was a loss of the image at bias settings more negative than 1 V and currents > 100 pA.

To acquire OMTS (dI/dV) spectra, bias modulation with lock-in detection was used. A modulation voltage of 50 mV at a frequency of 5 kHz was used. To remove the capacitive term in the dI/dV signal, the signal was offset.

D. Calculation Methods

The Gaussian 03[59] program was used to minimize the geometry and calculate the energy and wavefunctions for the free C_8 NDI. All calculations were performed using the 6-31+(d,p) basis method at the Hartree Fock level. Gaussview was used to generate the MO images and the optimized C_8 NDIs that are used to create the proposed monolayer structures on the STM images.

CHAPTER 3: RESULTS

3.1 TIP ANNEALING AND ETCHING

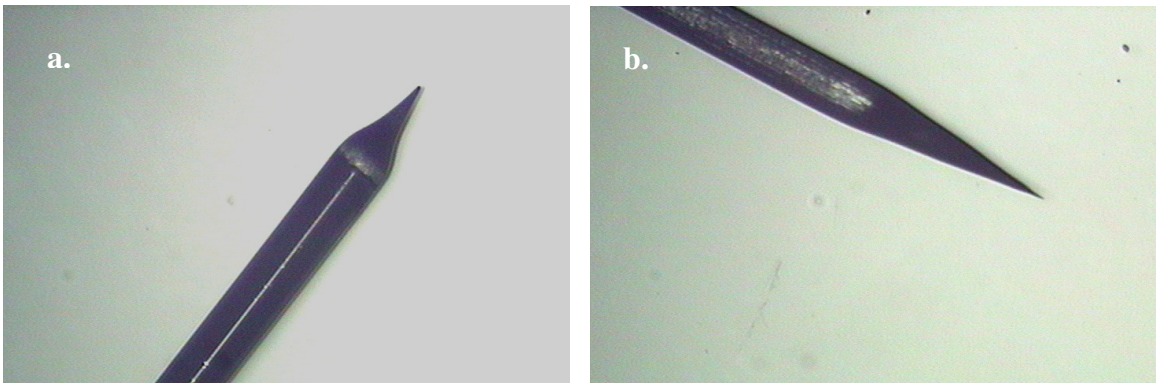

Figure 7: a.) PtIr etched at 25 V b.) Unannealed W tip

In the quest to find the sharpest, most reliable tips, unannealed W tips were first compared with PtIr tips. Figure 7 displays images of a PtIr tip and an unannealed W tip both etched at 25 V. While the PtIr tip has a well formed shaft, the tip seems to be blunt or in other words not atomically sharp to the human eye. The unannealed W tip on the other hand has a much longer shaft and to the eye seems much sharper. Several tips of both types were made to confirm the structures of the tips. Once it was confirmed that unannealed W gave the sharpest tips, different voltages were used to etch the unannealed W so as to improve the overall shape and reliability of the tips. Figure 8 compares

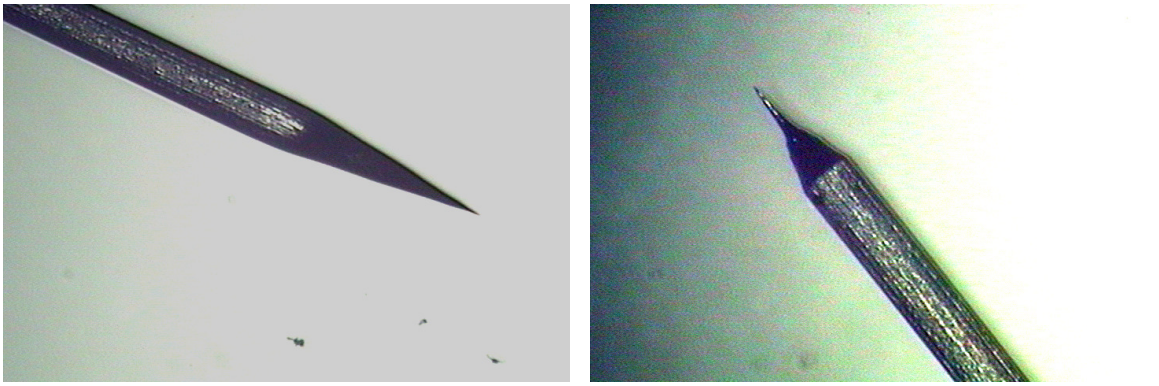

Figure 8: a.) Unannealed W at 25 V b.) Unannealed W at 5 V

unannealed W etched at 25 V and 5 V. At 25 V, the shaft of the tip is long and slowly tapers off, neither of which is a characteristic of a reliable tip. However, it can be seen that the tip is still sharp. At 5V the shaft is blunter closer to the unetched wire, but towards the tip, the shaft becomes thinner. The tip is still atomically sharp, however.

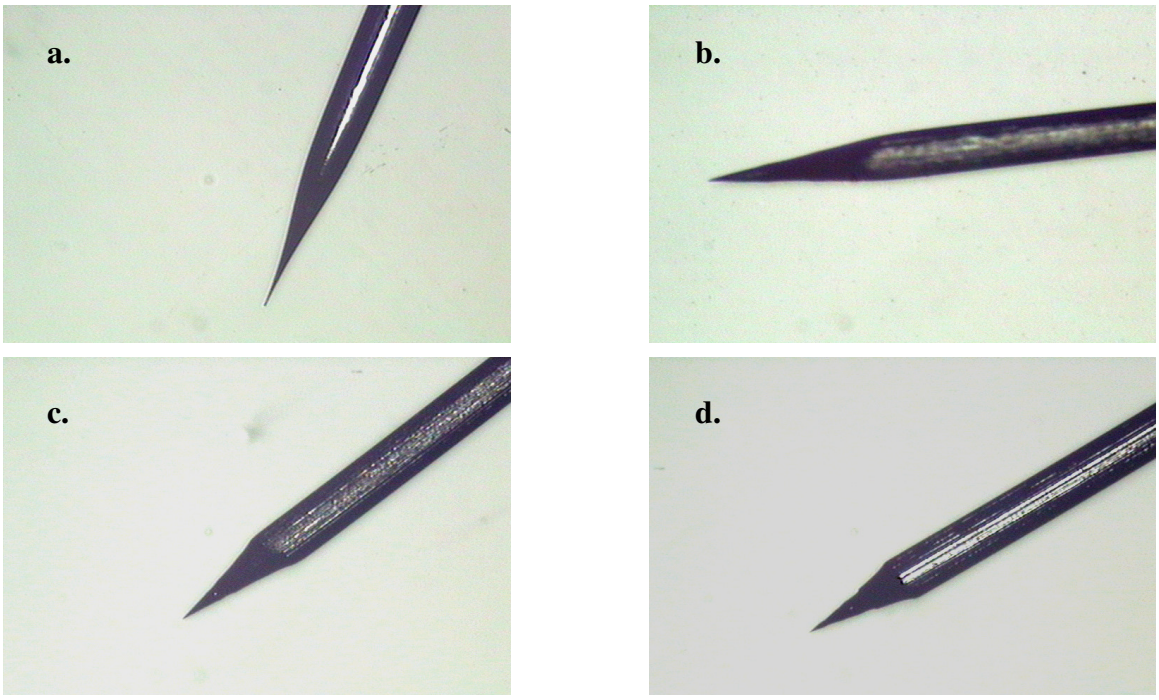

Figure 9: Annealed W tips etched at a.) 30 V b.)15 V c.) 7 V d.) 5V

In order to determine what parameters would produce the highest quality tips, annealed W was etched at various voltages. Figure 9 shows annealed W etched at 30 V, 15 V, 7V, and 5 V. The tip etched at 30 V has a long shaft that tapers off slowly as in Figure 8a. It also becomes thinner as it approaches the tip. This would make it unstable for imaging; however, the tip is still sharp to the naked eye. At 15 V the shaft structure is similar to that 30 V; however, the tip does not seem to be as sharp as it is at other voltages. At 7 V the tip begins to look like what would be considered an ideal tip structure. The shaft is relatively blunt and the tip is sharp. When the voltage was brought down to 5 V, the structure of the tip is relatively the same as those etched at 7V,

the main difference being that the shaft is a little bit shorter than the tip etched at 7 V. The 5 V setting was chosen as the ideal setting because its characteristics were most like those of an ideal and reliable tip.

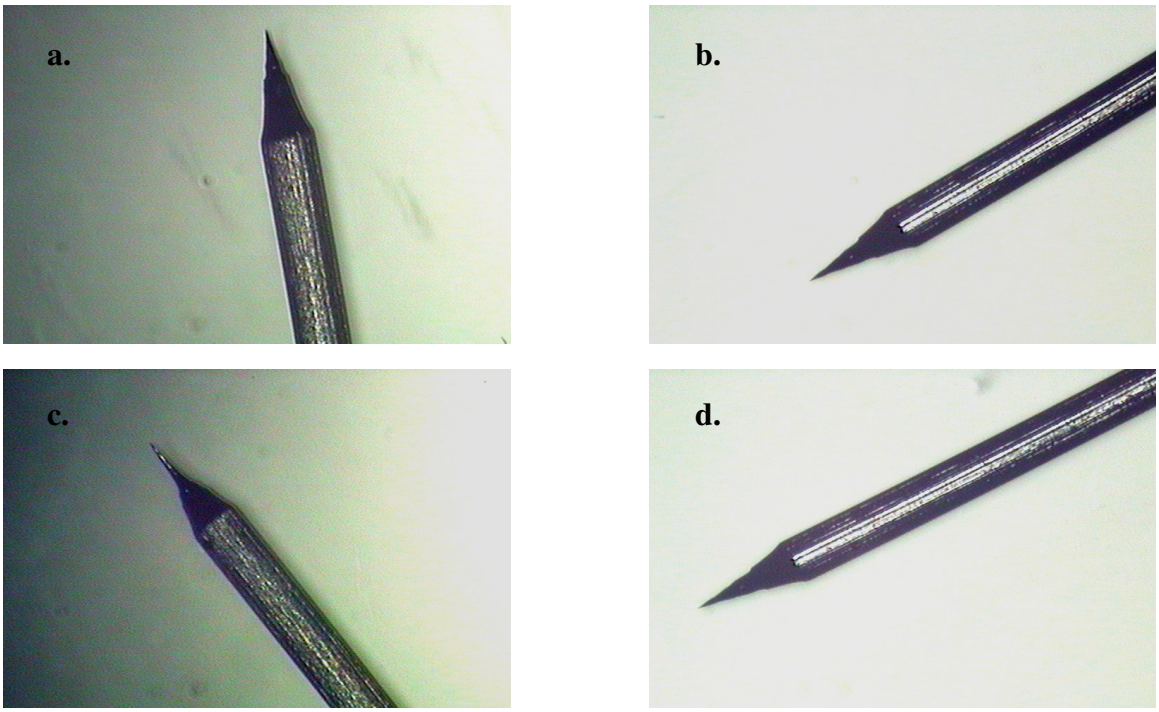

Figure 10: a.) and c.) Unannealed W tips etched at 5 V, b.) and d.) Annealed W tips etched at 5 V

Once it was determined that 5 V was the ideal setting to etch the annealed W at, it was decided that the unannealed W wire should also be etched at the same voltage. Figure 10 compares two trials of both the annealed and the unannealed W wire etched at 5 V. 10a. and c. are both unannealed W tips. Both trials reveal a blunt shaft with 10c. slowly tapering off to a sharp point and 10a. showing the same structure as that of an annealed tip etched at 5 V. Taking a look at the unannealed trials it can be seen that it is possible to etch tips with the ideal structure at 5 V; however, these trials also show that the shape of the tip is variable when using unannealed W wire. Looking at the annealed W wire trials in Figure 10b. and d., the tip structure is relatively consistent throughout.

The annealed W tips have the characteristics of having a blunt shaft and a sharp tip. What cannot be seen from Figure 10, but what is apparent when working with both the annealed and unannealed W wire, is the appearance and strength of the wire itself. When comparing the two types of wire, the annealed W wire has a much shinier appearance than the unannealed W wire. As far as the strength of each wire goes, the annealed W wire is much more brittle than the unannealed W wire. The annealed W wire can be split into two with just the pressure from a person's fingers, whereas the unannealed W wire requires scissors to cut it into half. When splitting the annealed W wire there is a clean break in the metal. The unannealed wire; however, splits like a banana peel at the point of the cut. Etching wire in this state can lead to multiple protrusions on the tip causing ghost images, otherwise known as a double tip image.

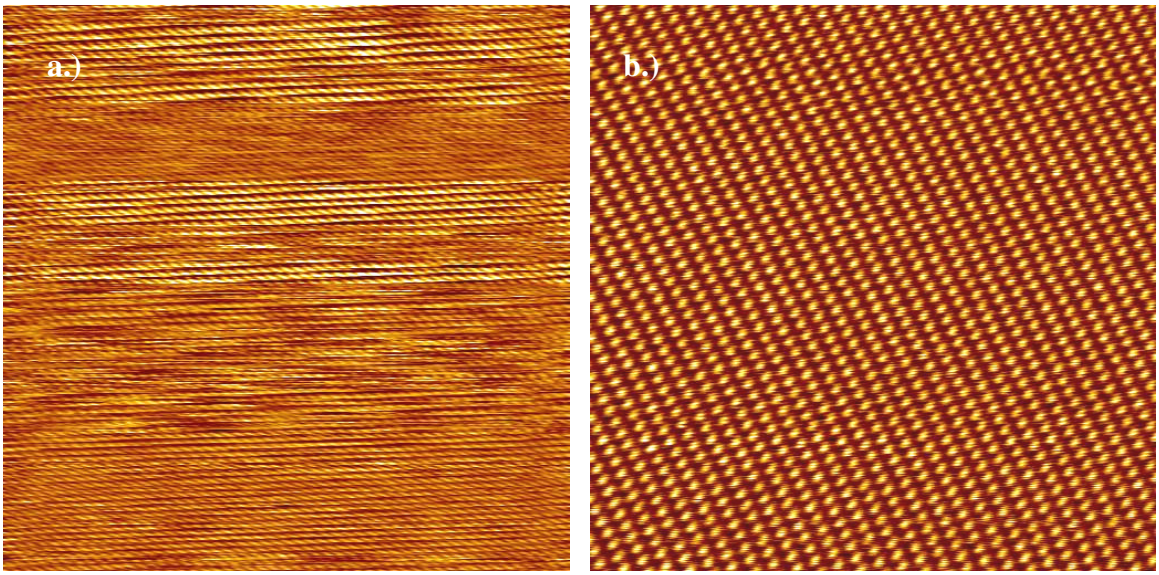

Figure 11: Constant Current STM of HOPG taken in air with a.) Unannealed W tip at 5 V b.) Annealed W Tip at 5 V Parameters: Scan Size: 10 nm, Setpoint: 725 pA, Bias Voltage: -95.91 mV, Scan Rate: 9.155 Hz

To determine whether the structure of the annealed W tips etched at 5 V really did provide better resolution images than the unannealed W tips etched at 5V, both types of

tips were used to scan a HOPG substrate at the same parameters. Figure 11 shows images of graphite taken with both the unannealed and annealed W wire at ambient conditions in air. There was a fair amount of noise in the image taken with the unannealed W tip (Figure 11a.). Also, the unannealed W tip gave poor resolution images. The annealed W tip on the other hand gave high resolution images with less noise than the unannealed W tips.

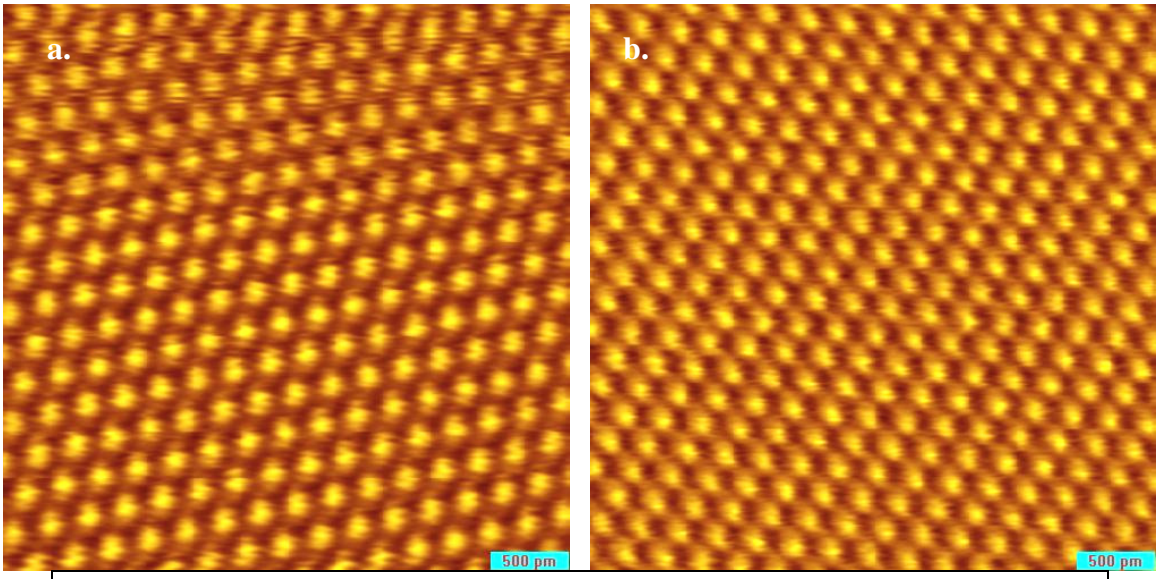

Figure 12: Constant Current UHV-STM images taken with Ar^+ sputtered annealed W tips sputtered for 1.5 min. at 25 mA and $5x10^{-5}$ torr.
a.) Etched at 5 V. Imaging: 0.100 V, 0.400 nA, 3.66 nm, 131 ms
b.) Etched at 7 V. Imaging: 0.400 V, 0.050 nA, 3.66 nm, 120 ms

In UHV, it is a common practice to ion sputter tips before using them to scan in order to get rid of any oxides or other contaminants that may have formed on the surface of the tip. The question is whether after being sputtered the tips are still sharp enough to give high resolution images. Figure 12 shows that in fact in both the cases of an annealed W tip being etched at 5 V and 7 V and then being argon ion sputtered, imaging was still successful. It is also apparent that the sputtering process did not cause the tips to loss their effectiveness in getting high resolution images.

3.2 STM OF NDIs

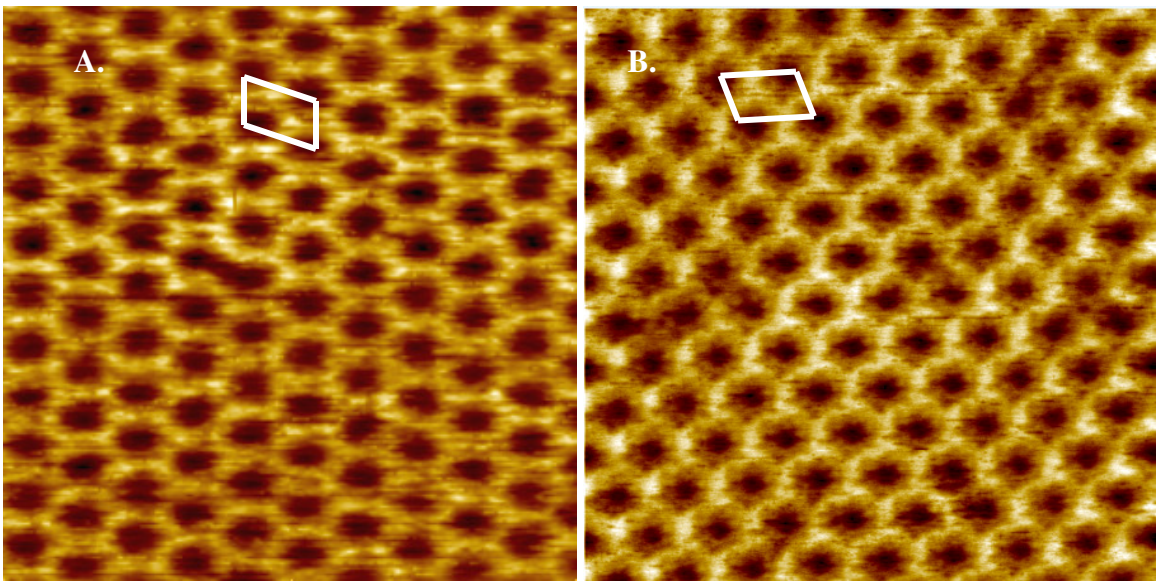

Figure 13: Constant Current STM images of a.) C_6 NDI in n-octylbenzene with unit cell. b.) C_{12} in toluene/n-octylbenzene with unit cell. Both images are 20 nm x 20 nm and were taken in ambient conditions.

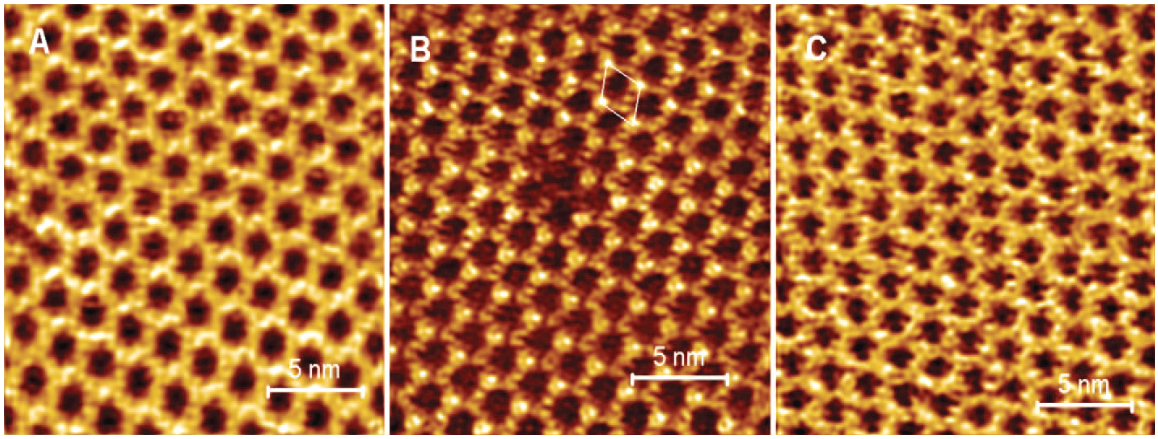

Figure 14: STM constant current images of the adlayer formed at the solution-HOPG interface at room temperature. (A) C_8 NDI in n-heptylbenzene, (B) C_8 NDI in n-octylbenzene, and (C) C_8 NDI in n-decylbenzene. Typical corrugation is 0.1 to 0.4 nm. A single unit cell is shown in B.[44]

All three NDIs were scanned in the STM at ambient conditions in air to determine their surface structure. It was found that all three NDIs have a pseudo-hexagonal

structure when adsorbed onto the HOPG surface. Figure 13 displays the typical results obtained for C_6 NDI in n-octylbenzene and C_{12} NDI in toluene/n-octylbenzene. Figure 14 shows the typical structure obtained for C_8 NDI in three of the five solvents used. In most of the images obtained, thermal drift was an issue. To combat thermal drift and get reliable lattice parameters, up and down scans were collected until the lattice analysis (with SPIP) in both directions was in reasonable agreement. Several up and down pairs were collected for each NDI (different samples, different tips, etc.) and the results were averaged to determine the unit cell of each NDI. The proposed unit cell parameters for each NDI are listed in Table 1. All unit cell parameters are within the same range with one another. Therefore, the unit cell structure is not affected by the length of the alkane substituted chain.

Sample	a	b	Angle
C_6 NDI in Solution	2.11± 0.04 nm	1.75 ± 0.14 nm	67.02 ± 2.39°
C_8 NDI in Solution	1.98± 0.25 nm	1.73 ± 0.25 nm	68.00 ± 2.00°
C_8 NDI Cast Film	1.97 ± 0.20 nm	1.95 ± 0.20 nm	66.00 ± 2.00º
C_{12} NDI in Solution	1.95 ± 0.10 nm	1.93 ± 0.09 nm	72.60 ± 2.60º

Table 1: Proposed unit cell parameters for C_6, C_8, and C_{12} NDI

To see what role, if any, solvents played in the unit cell structure of the NDIs, solutions of C_8 NDI were made in five different solvents and were deposited on HOPG. Figure 14 shows the results of three of those solvents. As can be seen from the data obtained, the changing of the solvent did not significantly affect the adlayer structure. This goes for all five solvents and all three NDIs. To minimize the presence of solvent molecules in the adlayer, a cast film was deposited on HOPG and the sample was transferred into the UHV-STM chamber. Before scanning the sample, it was annealed at 91°C for about 10 minutes at approximately $5x10^{-9}$ torr. Figure 15 displays constant current UHV-STM images of C_8 NDI. Both images were taken from the same area but several scans apart. As can be seen, even in a cast film sample, the adlayer structure is the same as the samples in solution. This is further conformation that solvents have a minor affect on the adlayer structure. After several measurements the unit cell for this sample was determined to be a=1.97±0.2 nm, b=1.95±0.2 nm, and α=66±2.0°. The images in Figure 15 were chosen because they contain defects created from missing molecules. Figure 15a. displays a defect resulting from one missing molecule. This area was repeatedly scanned and after several scans (at 15 pA and +1.5 V sample bias) the defect in Figure 15b. was what resulted. In this case, the defect now has two molecules missing. It is this type of evolution that clearly demonstrates that each of the small ring-like structures in the images are associated with a single NDI aromatic core. It also shows that these layers are very sensitive to tip-molecule interactions. In other systems studied in UHV,[36,39,42] such as porphyrins, phthalocyanines, and octyloxy species, scanning at higher currents and lower voltages did not affect the images significantly. However, in these systems, images of the adlayer structure could only be obtained using

low current and high voltage. This means that the tip has to be far from the surface in order for imaging to occur.

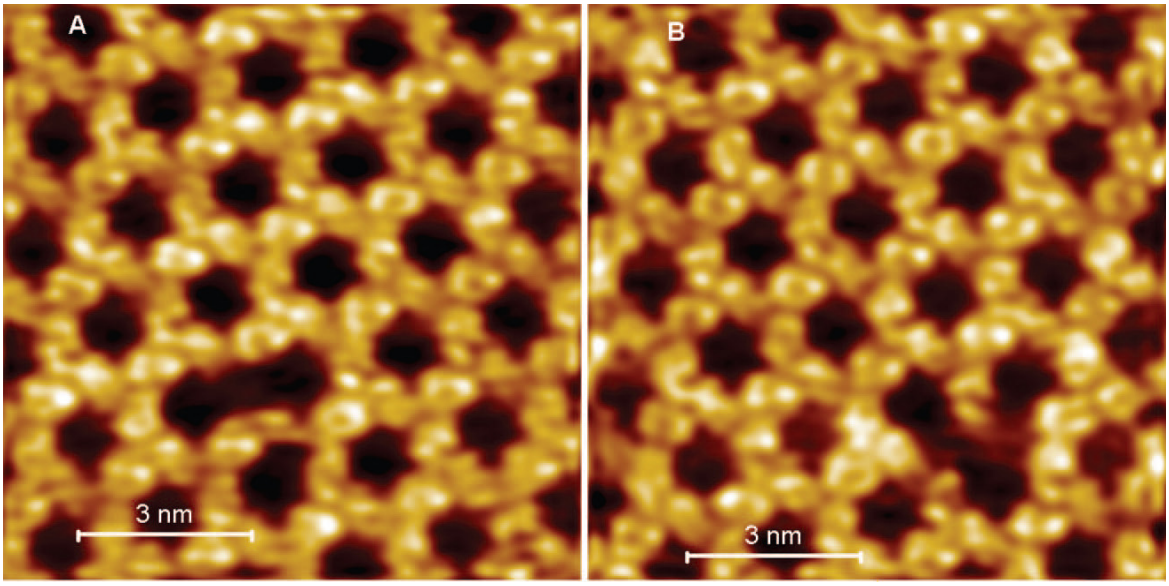

Figure 15: Constant current UHV STM image of diimide on HOPG. Diimide adsorbed from toluene and then annealed in UHV. Corrugation is 0.09 nm,1.5 V bias and 20 pA setpoint. Typical corrugation is 0.12 nm.[44]

3.3 ELECTRONIC STRUCTURE, I-V, AND OMTS OF C_8 NDI

SCF calculations were performed on the gas phase C_8 NDI with the octyl groups constrained in the plane of the aromatic ring. In order to determine its constrained equilibrium nuclear structure and its electronic structure, Gaussian03 was used to perform the calculations. Using the 6-31 G+(d,p) basis at the unrestricted Hartree Fock level, the first affinity level was found to be 1.5 eV below the vacuum level. The first ionization potential, on the other hand, was determined to be 8.6 eV for the gas phase, constrained planar, C_8 NDI. These values were compared to the literature. Seki et.al.[60] determined the first ionization potential for C_8 NDI on aluminum to be 8.7 eV using UPS and based on calculations found the affinity level to be 2.2 eV. If the first reduction potential in

solution is taken as an estimate[61,62] of the first affinity level,[42] then the first affinity level can be predicted to be about 4.2 eV. It is expected that the OMTS would contain bands near -3V (HOMO resonance) and +1.5 V (LUMO resonance),[42] based on UPS, electrochemical measurements and the assumption that the work function of the surface is 5 eV.

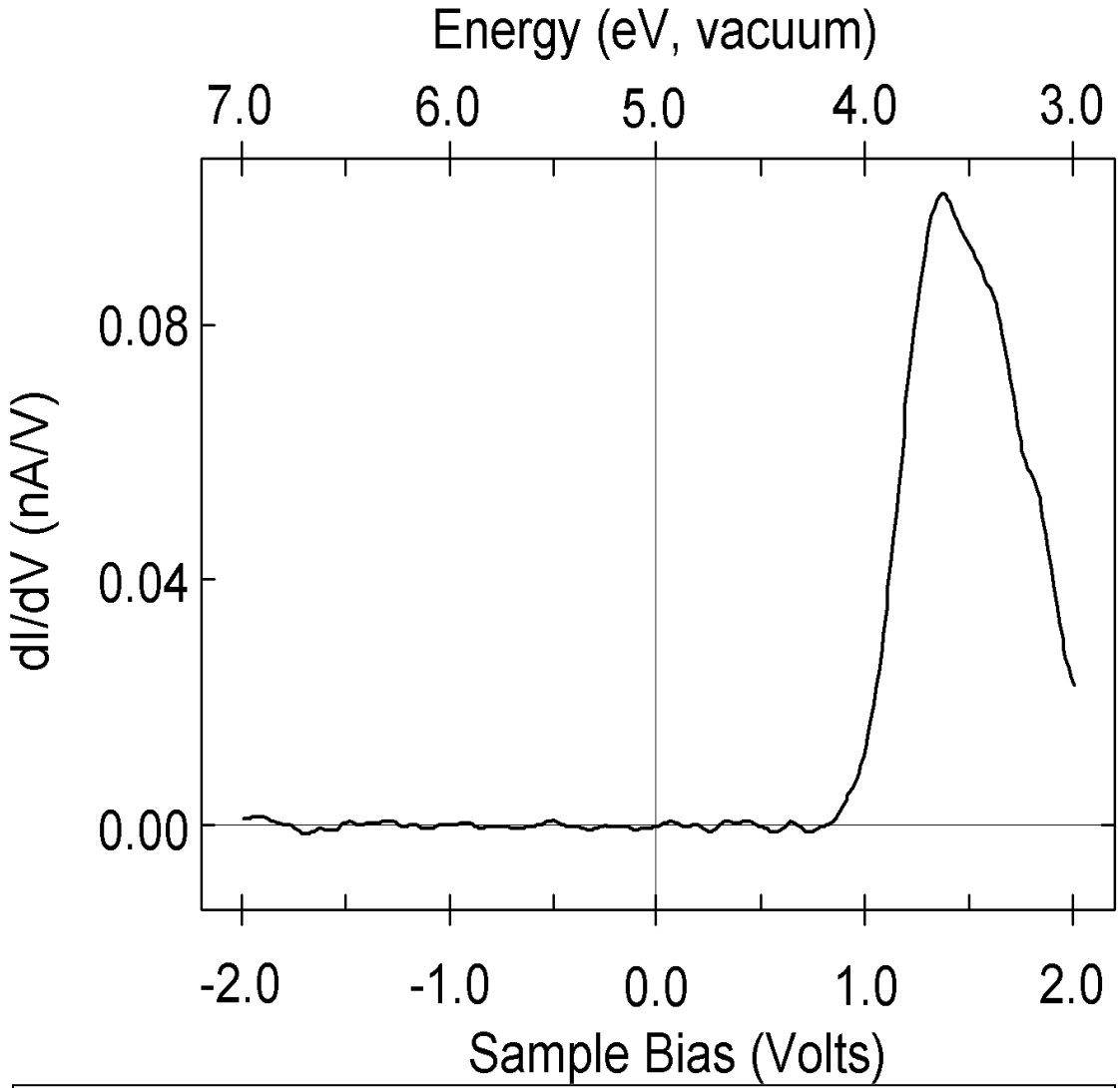

Figure 16: OMTS of the C_8 NDI taken in UHV. The upper energy scale was obtained by estimating the work function of the surface to be that of HOPG, 5.0 eV.[44]

Figure 16 displays the OMTS of C_8 NDI taken in UHV. It should be noted that the data range extends from -2 to +2 volts; therefore, the LUMO based electron affinity band at +1.4 V bias (about 3.6 eV below the vacuum level) is the only one that is seen. Figure 17 shows a current voltage curve of the C_8 NDI monolayer on HOPG. The C_8 NDI-HOPG surface shows very strong rectification resulting from the strong first electron affinity band with no corresponding ionization state within the voltage interval. The primary contrast mechanism (LUMO based tunneling) dramatically enhances the image of the ring rather than the alkane chains because the LUMO is localized on the ring.

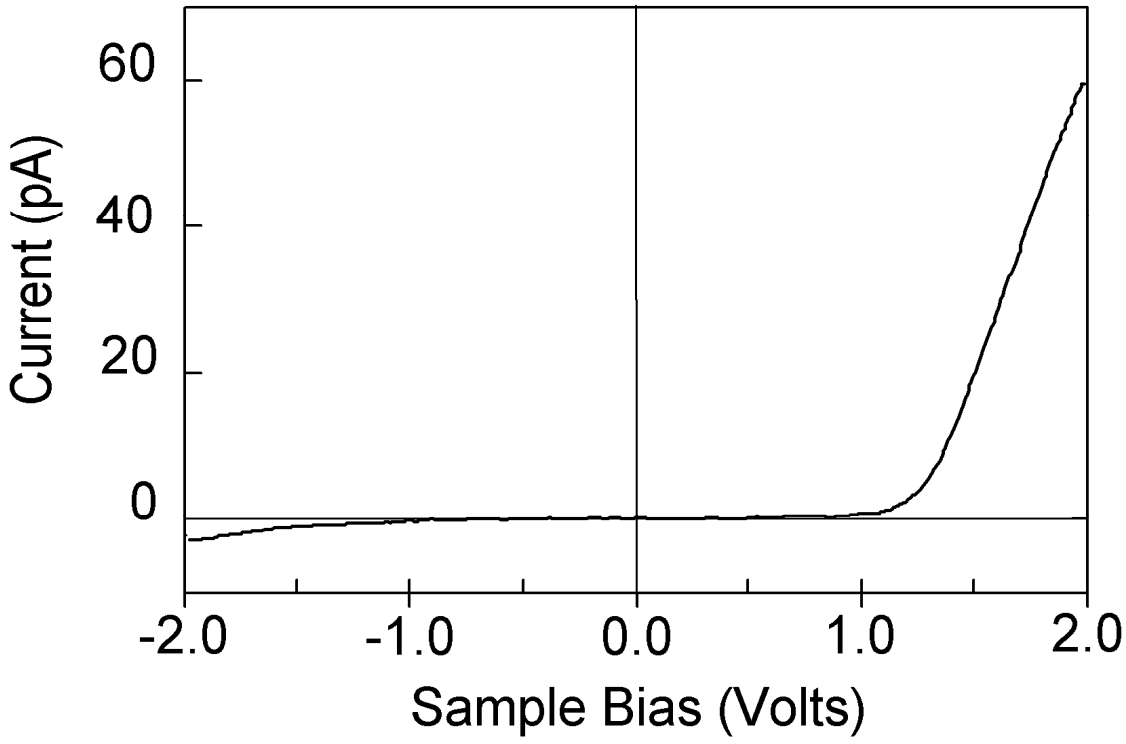

Figure 17: Current voltage curve of the C_8 NDI monolayer on HOPG taken in UHV.[44]

CHAPTER 4: DISCUSSION

4.1 PROPOSED MONOLAYER STRUCTURES

The structures observed for all three NDIs in Figures 13 and 14 are unlike those from most other alkane substituted systems. In most other linearly, alkane substituted aromatic systems, such as 4, 4'-bis(decyloxy)biphenyl and 4,4'-bis(hexadecyloxy)biphenyl the structure that is seen is linear or even rectangular. In a paper by Claypool et. al., structures where the adlayer was controlled by the alkane-HOPG interaction did not reproduce the observed NDI structures. To determine why the NDI structures are not like those of most other alkane substituted systems, SCF calculations performed on C_8 NDI were used. When the calculation was done at the 6-31G$^+$(d,p) SCF level, the alkane arms of the free molecule were at an angle of about 40° with the plane of the aromatic core. The calculated barrier for laying the arms flat was 8.8 kcal/mole per arm, which is similar to the heat of adsorption for octane on graphite (about 10 kcal/mol). Configuration changes may occur due to packing forces. Therefore, when fitting the molecules to the observed C_8 NDI structures, molecules with their octane arms lifted up from the surface were tried, as well as molecules with their octane arms laying flat on the surface.

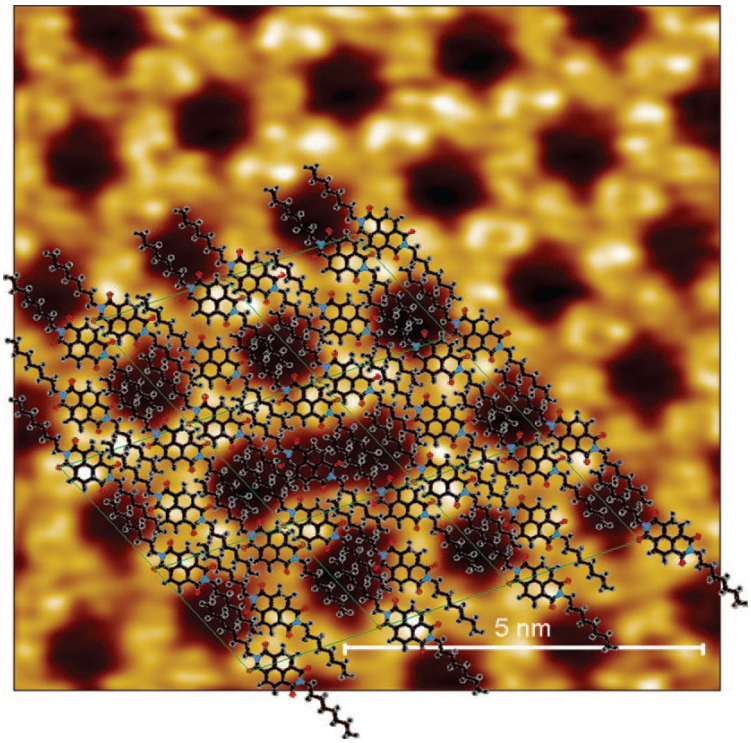

Figure 18: Overlay of monolayer structure with alkane arms lying flat and UHV-STM constant current image of C_8 NDI on HOPG.[44]

Figure 18 was the attempt made to reproduce the monolayer structure by laying the alkane arms of C_8 NDI flat on the surface of the graphite. This structure was created by requiring the cell dimensions to be equivalent to those that were experimentally observed in UHV. Also, the four C_8 NDIs at the corners were required to be equivalently related to the underlying lattice. The two remaining C_8 NDIs were placed somewhat arbitrarily within the cell to reproduce the STM image. Because of the alkane groups in the C_8 NDI, the structure that is shown in Figure 18 is rather crowded. It is easy to imagine that if the C_8 NDI was replaced with the C_6 NDI, the same structure, if not roomier, would result if the arms were to lay flat on the surface. C_8 NDI would be more crowded than C_6 NDI due to the length of the alkane arms. However, as the alkane chains get longer, as in the case of C_{12} NDI, the proposed structure for C_8 NDI with the

arms laying flat on the surface of the HOPG, no longer works due to overcrowding. A more likely structure is one where the alkane arms leave the graphite surface, as is the case of studies done by Kaneda et. al.[21], Stawasz et. al.[22], and Tahara et. al.[25].

All three studies are alkane substituted aromatic systems adsorbed on HOPG in which, in order to account for some of the monolayers seen, the alkane arms left the surface of the graphite. The study by Kaneda and coworkers[21] is of particular interest because it was performed on a set of molecules related to our own. Kaneda and coworkers[21] performed STM on Perylenetetracarboxylic acid N-Alkyl-diimides (PTCDI) on HOPG. They found for all five systems (C_4, C_8, C_{12}, C_{13}, and C_{18} PTCDI) they studied what they call a rectangular polytype where the alkane arms were desorbed from the surface. The measured molecular areas for each of the molecules did not change with alkane chain length. They concluded from this that the interaction between the PTCDI core and the graphite surface was what drove the monolayer structure, and therefore, the alkane arms had no effect on the monolayer structure.

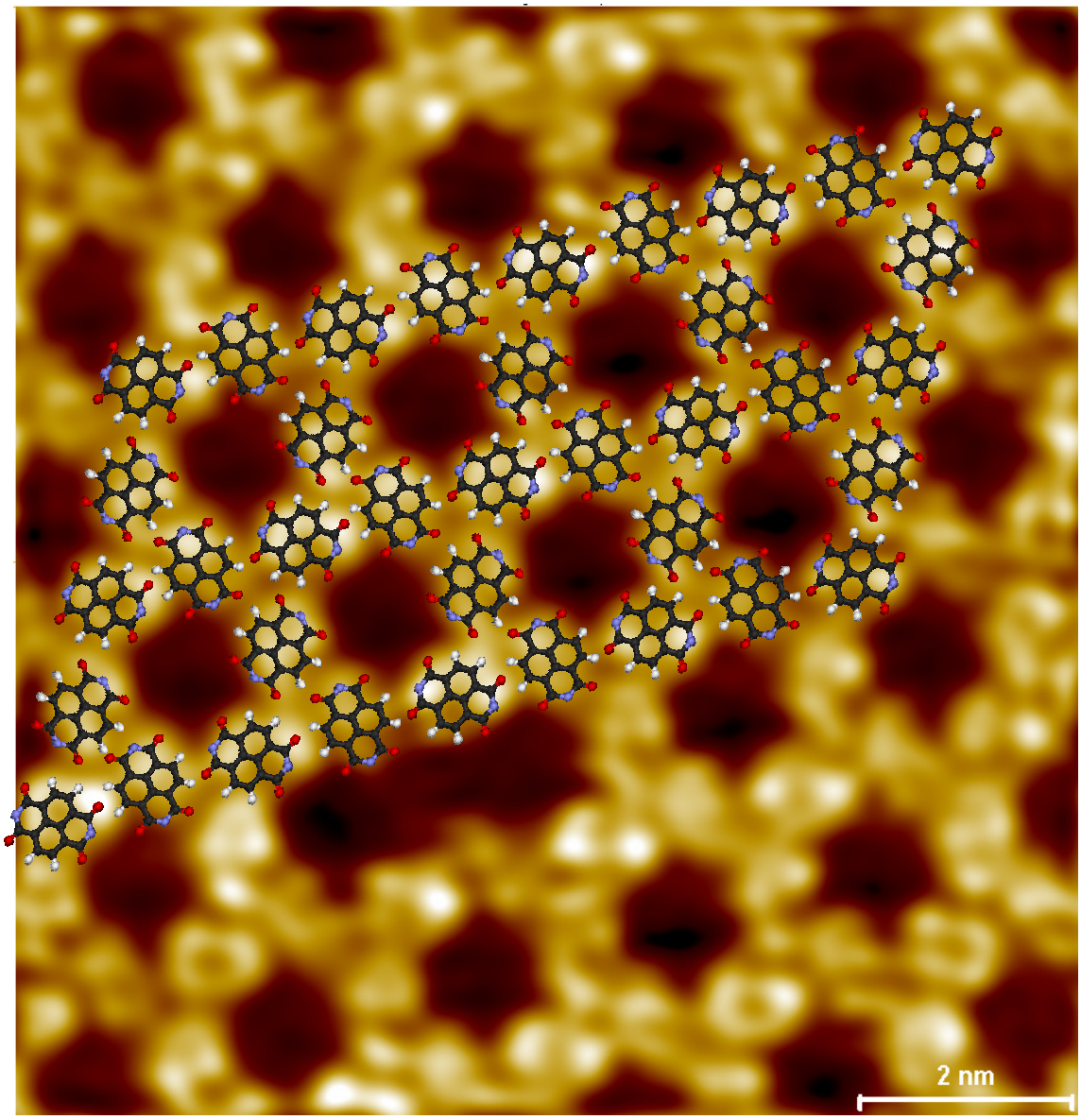

Figure 19: Overlay of proposed monolayer structure with alkane arms desorbed from surface and UHV-STM constant current image of C_8 NDI cast film on HOPG.

Knowing that there was no way the C_{12} NDI structure could be reproduced with the alkane arms lying flat on the graphite surface, we proceeded by fitting the NDI core to the C_8 NDI UHV-STM image (Figure 19). Only the NDI core was fitted because it was assumed that the alkane arms were desorbed from the surface, and based on the SCF calculations mentioned before, the minimum energy in the gas phase for C_8 NDI occurs

when the alkane arms are pointed out of the NDI core plane by about 40°. Because of this, energy wise it is not costly to use C-C rotations to reduce steric problems. It was also noticed that in both UHV and air, the samples were scanned at low current (+7-+20 pA) and high voltages (+1.00-+1.50 V), which suggests that the tip needs to be far from the sample surface in order for imaging to occur. The fact that the tip is far from the surface, further suggests that the arms are out of the NDI core plane and could be interfering with the tip-surface interaction. It is likely that the tip has to be far from the surface because the alkane arms are sticking out into the solution and the only way to get any kind of resolution is to avoid the arms by being far from the surface. The use of the NDI cores for the overlaying of the monolayer structure on the image is further supported by these observations.

In order to determine how to fit the NDI cores to the image, the defect in the image was associated with one missing molecule and it was assumed that each bright spot was associated with one NDI core. With this information, NDI cores were positioned by placing one NDI core on top of each bright spot on the image. The cores could not be positioned facing the same angle because the oxygens, nitrogens and alkane arms would be directly interacting with one another. The NDI cores were therefore rotated at three different angles to minimize the interactions between the oxygens, nitrogens and alkane arms, but still reproduce the monolayer structure. After fitting the ball and stick NDI cores to the UHV-STM image, CPK models of the NDI core were

fitted to the image to see how the atoms interact with one another.

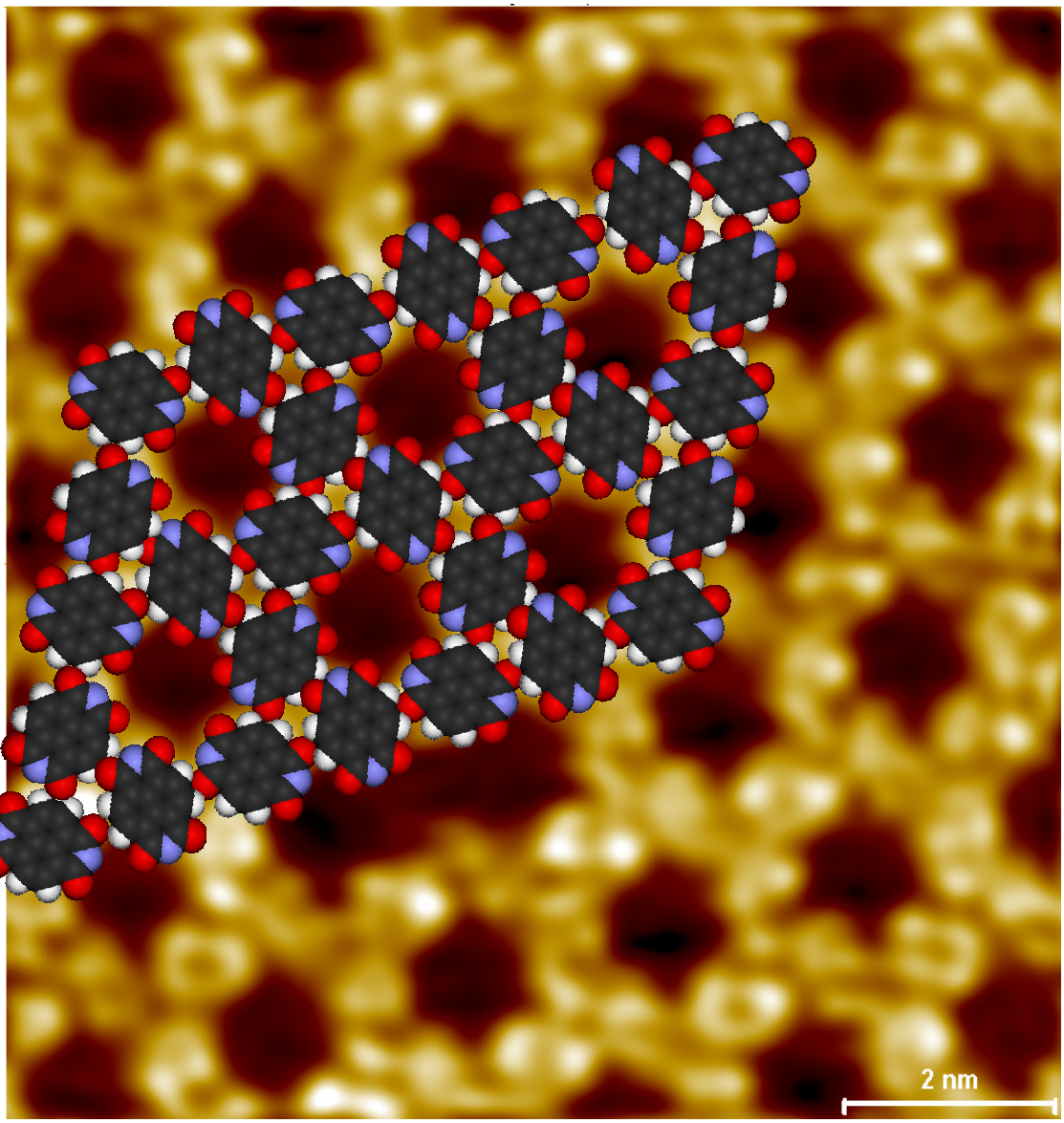

Figure 20: Overlay of CPK proposed monolayer structure with alkane arms desorbed from surface and UHV-STM constant current image of C_8 NDI cast film on HOPG.

Figure 20 shows the resulting monolayer structure overlaid on the image. It can be seen from this image just how tight the molecules are packed in the structure. This leaves little room for the alkane chains to fit anywhere. It is important, however, to mention that the CPK models are an estimate of the size of the atoms, and as such, the radiuses could

be smaller or even larger. Also thermal drift may contribute to the overlaid CPK monolayer structure not being completely in line with the underlying structure. The CPK model still shows, however, that just fitting the NDI cores leaves little room for the alkane chains in the structure and it is this that further supports the theory that the arms must be lying at an angle to the plane of the NDI core.

Once an acceptable monolayer structure was found for the C_8 NDI system in UHV, we proceeded on to the C_6, C_8 and C_{12} NDI systems in solution using the same monolayer structure. The monolayer structure for the C_8 NDI cast film should have been able to be used to reproduce the images of all three NDI systems. However, due to the quality of the images used and the amount of drift in each of the images, there was difficulty in producing acceptable monolayer structures on each of the systems in solution. In the case of the C_8 NDI cast film, the image used was taken in UHV (Figure 19 and 20). The C_6, C_8 and C_{12} NDI systems in solution were imaged in air at ambient conditions. In UHV, higher resolution images can be obtained when compared to imaging done in air. This is partly due to the amount of thermal drift during scanning. The UHV system is in a controlled environment. In air, the system is more susceptible to changes in climate and concentration, making it more prone to thermal drift and causing the unit cell to be skewed. Another reason why the unit cells may be skewed when compared to one another is that it is possible that part of the alkane chains still interact with the graphite surface, making the unit cells slightly different for each of the systems. Kaneda and coworkers[21] theorized this possibility for the PTCDI systems. All these factors lead to differences in the type of resolution and unit cells obtained. This being the case, it is possible that if better resolution images of C_6, C_8 and C_{12} NDI in solution could

be obtained, a better correlation between the overlaid proposed monolayer structure from UHV and the actual structure in the images would also be seen.

4.2 SURFACE STRUCTURE RELATIVE TO GRAPHITE

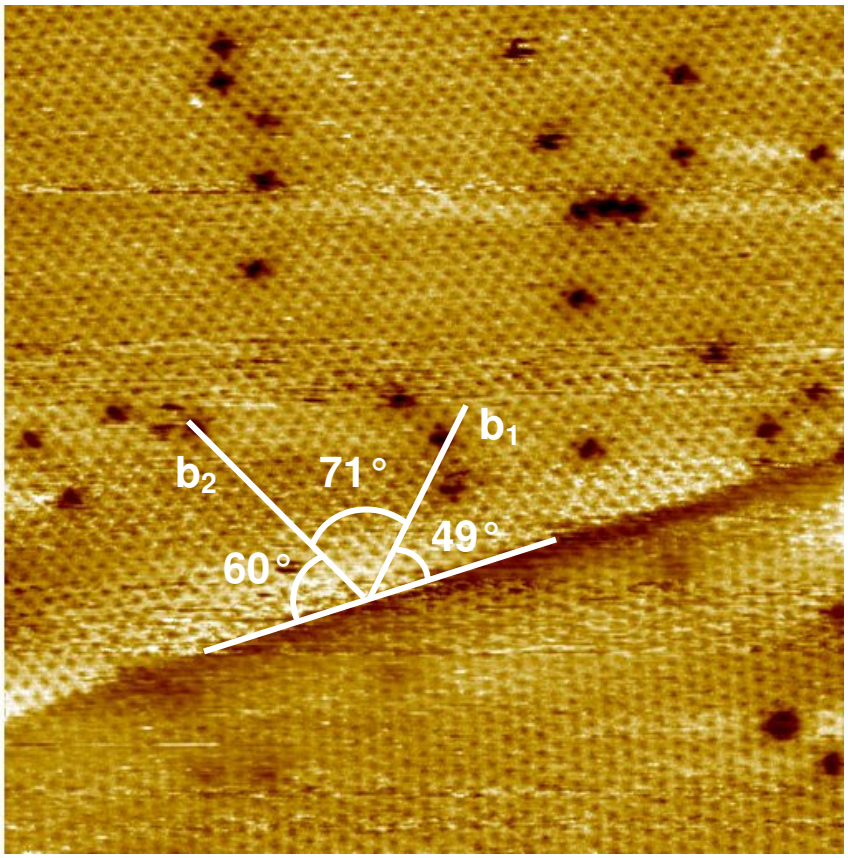

Figure 21: Constant Current STM image of C_{12} NDI in toluene/n-octylbenzene. Unit cell vectors for b_1 and b_2 are shown, along with angles relative to the HOPG step edge.

In order to determine the orientation of the NDI monolayers relative to the HOPG surface, images of the monolayers along a step edge of HOPG were obtained. C_{12} NDI was the only system in which images with enough resolution along the step edge could be obtained for these studies; therefore, this is the system that will be discussed. Once

acceptable images were obtained, a straight line is drawn across the step edge as can be seen in Figure 21. The two different angles and directions of the monolayer structure relative to the step edge are then found. In this case, there is a b_1 and b_2 vector and their angles relative to the step edge are 49° and 60° respectively. Once this information is determined, the vectors and their angles are transferred to hexagonal graphite lattice sheet, as can be seen in Figure 22.

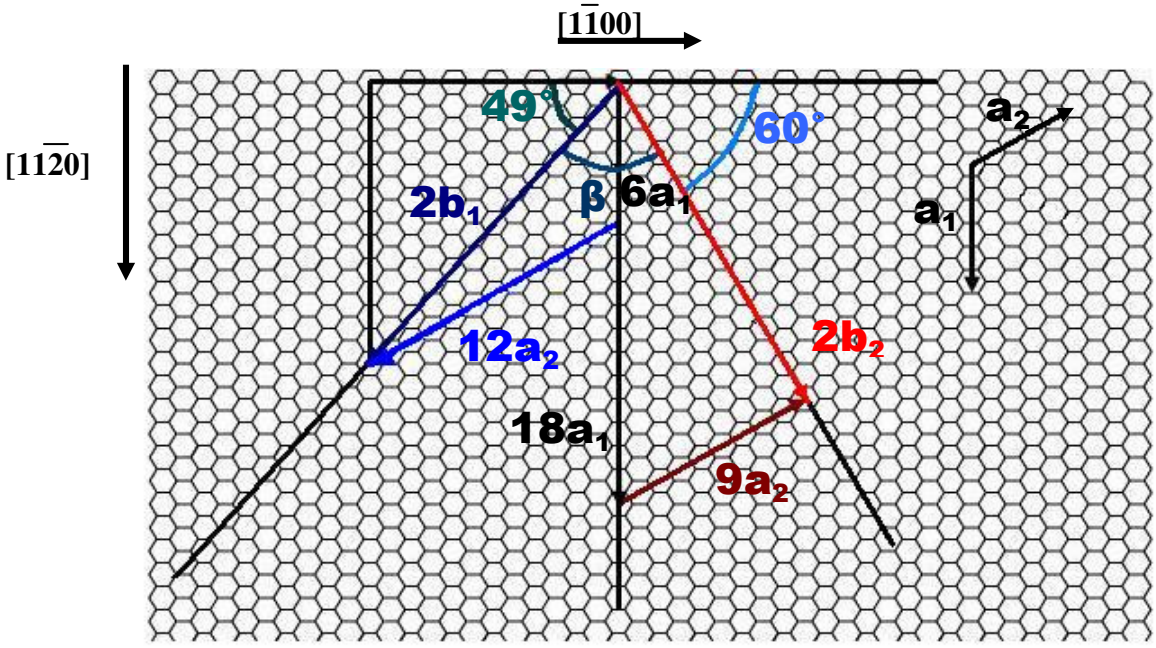

Vector Equations	Length of Vector	Angle of Vector
$b_1=3a_1 - 6a_2$	b_1=1.95 nm	49°
$b_2=9a_1 + (9/2)a_2$	b_2= 1.92 nm	60°
Angle of Unit Cell	β= 71°	

Figure 22: Unit Cell and Unit Cell Parameters of C_{12} NDI relative to step edge of HOPG.

The unit vectors are drawn in such a way as to match the experimentally observed unit cell. In this case, both b vectors are drawn twice their actual length to make the calculations simpler. From this point, the a vectors are drawn in such a way as to connect with the b vectors and from here the b vector equations can be determined by determining

the length of both a vectors. Taking the values of the b_1 equation and inserting them into the equation, $c^2=a^2+b^2-2abcos\theta$, where a and b are the lengths of your a vectors and cosθ is taken as the cos 60=0.5, then dividing that answer by two, the b_1 vector length is determined to be 1.95 nm. For b_2, the vector length is easier to determine because it is going in a point on line coincidence direction. All that needed to be done in this case was to take the length relative to the graphite lattice of the line drawn for twice the b_2 vector and multiply that by √(3) a, where √(3) is the number of periodicity and a is the unit cell length of the substrate (a=0.246 nm for HOPG). This value is then divided by two because the b_2 vector drawn was twice the length of the actual b_2 vector. The b_2 vector length was determined to be 1.92 nm. Finally, the angles of vectors relative to the step edge were checked using geometry and from there the internal angle of the unit cell was found to be β=71°.

When compared to actual experimental data, the values obtained from determining the structure surface of the monolayer relative to the graphite are almost identical to the experimental data. The experimental unit cell parameters for C_{12} NDI in solution were a=1.95 ± 0.10 nm, b=1.93 ± 0.09 nm, and α=72.60 ± 2.60º. The unit cell parameters obtained from surface structure relative to the graphite are b_1=1.95 nm, b_2=1.92 nm, and β=71°. This gives further conformation that the unit cell seen experimentally is the correct unit cell for C_{12}. The next step in the process would be to determine how the molecules actually lay across the top of the graphite surface and in what directions. Further information is needed to determine the exact orientation of the molecules.

CHAPTER 5: CONCLUSION

In this study it was found that when compared to PtIr tips, there is a noticeable difference in the macrostructure of tungsten tips. It was also found that unannealed W wire is less reflective than annealed W and that the annealed W wire is more brittle than the unannealed W wire. This suggests that the annealed W wire is more crystalline than the unannealed. It was found that 5 V was the best etching voltage from the voltages tested to use in order to meet the requirements of a reliable tip. Imaging was possible with both annealed and unannealed tips, but annealed tips have a much higher rate of success giving good images. When the tips were used in ultra-high vacuum, the sputtering process did affect the reliability of the tip. It improved the signal to noise ratio and the IV curve. Also, it left the tip sufficiently sharp to take images.

As for the STM studies, C_6, C_8, and C_{12} NDIs were successfully imaged on HOPG. Unlike other alkane substituted systems where the monolayers consisted of ordered rows of molecules with the spacing of the rows determined by the length of the chains, the structure of the NDI monolayers is pseudo-hexagonal and seems to be dependent on the core NDI-HOPG interactions. Because all three NDIs have the same structure and similar unit cell parameters, the length of the alkane chains substituted on the NDI has little effect on the structure of the monolayer. In the case of C_8 NDI this would mean that the alkane chains would have to be sticking up at an angle from the NDI core to reproduce the same structural results as C_6 and C_{12} NDI. This supports the theory that the NDI monolayer structure is dependent on the core NDI-HOPG interactions. Further study is needed to determine if this is in fact the case. Better resolution images of

these three NDIs using cast films and NDIs substituted with other functional groups could give further clues as to the behavior of NDIs on the surface of graphite. Also the use of an unsubstituted NDI in these studies may provide valuable information as to whether or not the adlayer structure is strictly dependent on the interaction between the NDI core and the HOPG surface.

The surface structure for C_{12} NDI was determined relative to the underlying graphite structure. It was found that the unit cell obtained from these calculations were almost exactly the same as the unit cell that is experimentally observed, providing us with further clues as to the interaction between the graphite surface and the monolayers. Higher resolution images of the C_6 and C_8 NDI systems along graphite edges are needed to determine their surface structure relative to the graphite surface. Further studies, such as placing the NDI cores over the graphite lattice, could give more information on the interactions between the NDI cores and the graphite lattice and be used to figure out how the underlying HOPG drives the formation of the monolayer.

The OMTS of C_8 NDI revealed that the first ionization level was deeper than 7.0 V below the vacuum level and that the first affinity level was near 3.5 V below the vacuum level. Constant Current STM images of the NDI monolayers revealed that they were dominated by LUMO tunneling, which caused the core rings to appear bright while the octane chains were nearly invisible. There was a great loss of corrugation for sample bias voltage between -1.8 and +1.0 V in bias voltage dependent images in air and in vacuum. With further investigation into the OMTS of the C_6 and C_{12} NDI systems, more information may be obtained regarding the electronic structures of these systems and how they affect the formation of monolayers on the HOPG surface.

REFERENCES

[1] Giancarlo, L.C.; Fang, H.; Avila, L.; Fine, L.W.; Flynn, G.W. *J. Chem. Ed.* **2000**, *77*, 66-71.

[2] Hansen, T.; Itoua, S.; Kamounah, F.; Christensen, J.B.; Bjornholm, T.; Schaumburg, K.; Bechgaard, K.; Wilkes, S.B. *J. Mater. Chem.* **1999**, *9*, 1107-1113.

[3] Wolpaw, A.J.; Aizer, A.A.; Zimmt, M.B. *Tetrahedron Letters* **2003**, *44*, 7613-7615.

[4] Claypool, C.L.; Faglioni, F.; Matzger, A.J.; Goddard, W.A., III; Lewis, N.S. *J. Phys. Chem. B.* **1999**, *103*, 9690-9699.

[5] Patrick, D.L.; Cee, V.J.; Morse, M.D.; Beebe, T.P., Jr. *J. Phys. Chem. B*. **1999**, *103*, 8328-8336.

[6] Yablon, D.G.; Giancarlo, L.C.; Flynn, G.W. *J. Phys. Chem. B*. **2000**, *104*, 7627-7635.

[7] Zhu, Y.J.; Hansen, T.A.; Ammermann, S.; McBride, J.D.; Beebe, T.P., Jr. *J. Phys. Chem. B* **2001**, *105*, 7632-7638.

[8] Samori, P.; Jackel, F.; Unsal, O.; Godt, A.; Rabe, J.P. *Chem. Phys. Chem*. **2001**, *2*, 461-464.

[9] Wei, Y.; Kannappan, K.; Flynn, G.W.; Zimmt, M.B. *J. Amer. Chem. Soc.* **2004**, *126*, 5318-5322.

[10] Piot, L.; Marchenko, A.; Wu, J.; Müllen, K.; Fichou, D. *J. Amer. Chem. Soc.* **2005**, *127*, 16245-16250.

[11] Tao, F.; Bernasek, S.L. *J. Phys. Chem. B* **2005**, *109*, 6233-6238.

[12] De Feyter, S.; De Schryver, F.C. *J. Phys. Chem. B* **2005**, *109*, 4290-4302.

[13] Hulsken, B.; Van Hameren, R.; Thordarson, P.; Gerritsen, J.W.; Nolte, R. J.M.; Rowan, A.E.; Crossley, M.J.; Elemans, J.A.A.W.; Speller, S. *Japanese Journal of Applied Physics*, **2006**, *45*, 1953-1955.

[14] Oiu, X.; Wang, C.; Yin, S; Zeng, Q.; Xu, B.; Bai, C. *J. Phys. Chem. B* **2000**, *104*, 3570-3574.

[15] Zhou, Y.; Wang, B.; Zhu, M.; Hou, J.G. *Chem. Phys. Lett.* **2005**, *403*, 140-145.

[16] Mourran, A.; Ziener, U.; Möller, M.; Breuning, E.; Ohkita, M.; Lehn, J.M. *European Journal of Inorganic Chemistry* **2005**, 2641-2647.

[17] Wang, H.; Wang, C.; Zeng, Q.; Xu, S.; Yin, S.; Xu, B.; Bai, C. *Surface and Interface Analysis* **2001**, *32*, 266-270.

[18] Kikkawa, Y.; Koyama, E.; Tsuzuki, S.; Fujiwara, K.; Miyake, K.; Tokuhisa, H.; Kanesato, M. *Langmuir* **2006**, *22*, 6910-6914.

[19] Klymchenko, A.S.; Sleven, J.; Binnemans, K.; De Feyter, S. *Langmuir* **2006**, *22*, 723-728.

[20] Abdel-Mottaleb, M.M.S.; Gomar-Nadal, E.; Surin, M.; Uji-I, H.; Mamdouh, W.; Veciana, J.; Lemaur, V.; Rovira, C.; Cornil, J.; Lazzaroni, R.; Amabilino, D.B.; De Feyter, S.; De Schryver, F.C. *Journal of Materials Chemistry* **2005**, *15*, 4601-4615.

[21] Kaneda, Y.; Stawasz, M.E.; Sampson, D.L.; Parkinson, B.A. *Langmuir* **2001**, *17*, 6185-6195.

[22] Stawasz, M.E.; Sampson, D.L.; Parkinson, B.A. *Langmuir* **2000**, *16*, 2326-2342.

[23] Wu, P.; Zeng, Q; Xu, S.; Wang, C.; Yin, S.; Bai, C.L. *ChemPhysChem* **2001**, *12*, 750-754.

[24] Mamdouh, W.; Uji-I, H.; Ladislaw, J.S.; Dulcey, A.E.; Percec, V.; De Schryver, F.C.; De Feyter, S. *J. Amer. Chem. Soc*. **2006**, *128*, 317-325.

[25] Tahara, K.; Furukawa, S.; Uji-I, H.; Uchino, T.; Ichikawa, T.; Zhang, J.; Mamdouh, W.; Sonoda, M.; De Schryver, F.C.; De Feyter, S.; Tobe, Y. *J. Amer. Chem. Soc*. **2006**, *128*, 16613-16625.

[26] Tao, F.; Goswami, J.; Bernasek, S.L. *J. Phys. Chem. B*. **2006**, *110*, 19562-19569.

[27] Venkataraman, B.; Breen, J.J.; Flynn, G.W. *J. Phys. Chem.* **1995**, *99*, 6608-6619.

[28] Kampschulte, L.; Lackinger, M.; Maier, A.K.; Kishore, R.S.K.; Griessl, S.; Schmittel, M.; Heckl, W.M. *J. Phys. Chem. B.* **2006**, *110*, 10829-10836.

[29] Gyarfas, B.; Wiggins, B.; Zosel, M.; Hipps, K.W. *Langmuir*, **2005**, *21*, 919-923.

[30] (a) Stevens, F.; Dyer, D. J.; Walba, D. M. *Langmuir* **1996**, *12*, 436. (b)Hipps, K. W.; Lu, X.; Wang, X. D.; Mazur, U. *J. Phys. Chem*. **1996**, *100*, 11207. (c) Baker, R. T.; Mougous, J. D.; Brackley, A.; Patrick, D. L. *Langmuir* **1999**, *15*, 4884. (d) Padowitz, D. F.; Sada, D. M.; Kemer, E. L.; Dougan, M. L.; Xue, W. A. *J. Phys. Chem. B* **2002**, *106*, 593. (e) De Feyter, S.; Larsson, M.; Schuurmans, N.; Verkuijl, B.; Zoriniants, G.; Gesquie`re, A.; Abdel-Mottaleb, M. M.; van Esch, J.; Feringa, B. L.; van Stam, J.; De Schryver, F. C. *Chem.*s *Eur. J*. **2003**, *9*, 198.

[31] De Feyter, S.; Gesquie`re, A.; Abdel-Mottaleb, M. M.; Grim, P. C. M.; De Schryver, F. C.; Meiners, C.; Sieffert, M.; Valiyaveettil, S.; Mu¨llen, K. *Acc. Chem. Res*. **2000**, *33* (8), 520-531.

[32] Theobald, J. A.; Oxtoby, N. S.; Philips, M. A.; Champness, N. R.; Beton, P. H. *Nature* **2003**, 424, 1029-1031.

[33] Scherer, L.J.; Merz, L.; Constable, E.C.; Housecroft, C.E.; Neuburger, M.; Hermann, B.A. *JACS* **2005**, *127*, 4033-4041.

[34] Yin, X.L.; Wan, L.J.; Yang, Z.Y.; Yu, J.Y. *Appl. Surf. Sci.* **2005**, *240*, 13-18.

[35] Ogunrinde, A.; Hipps, K.W.; Scudiero, L. *Langmuir* **2006**, *22*, 5697-5701.

[36] Pokrifchak, M.; Turner, T.; Pilgrim, I.; Johnston, M.R.; Hipps, K.W. *J. Phys. Chem. C.* **2007**, *111*, 7735-7740.

[37] (a)Griessl, S.H.; Lackinger, M.; Edelwirth, M.; Hietschold, M.; Heckl, W.M. *Single Mol.* **2002**, *3*, 25. (b) Griessl, S.H.; Lackinger, M.; Fjamitzky, F.; Markert, T.; Hietschold, M.; Heckl, W.M. *J. Phys. Chem. B*. **2004**, *108*, 11556.

[38] Hecht, S. *Angewandte Chemie, International Edition* **2003**, *42*, 24.

[39] Hipps, K.W.; Scudiero, L.; Barlow, D.E.; Cooke, M.P. *J. Amer. Chem. Soc.* **2002**, *124*, 2126.

[40] De Feyter, S.; De Schryver, F.C. *Chemical Society Reviews* **2003**, *32*, 139.

[41] Schenning, A.P.H.J.; Jonkheijm, P.; Hoeben, F.J.M.; Van Herrikhuyzen, J.; Meskers, S.C.J.; Meijer, E.W.; Herz, L.M.; Daniel, C.; Silva, C.; Phillips, R.T.; Friend, R.H.; Beljonne, D.; Miura, A.; De Feyter, S.; Zdanowska, M.; Uji-I, H.; De Schryver, F.C.; Chen, Z.; Wuerthner, F.; Mas-Torrent, M.; Den Boer, D.; Durkut, M.; Hadley, P. *Synthetic Metals* **2004**, *147*, 43.

[42] Hipps, K.W. In "*Handbook of Applied Solid State Spectroscopy*", Vij, D.R., Ed,; Springer Verlag: New York, **2006**, p.305.

[43] Hipps, K.W.; Scudiero, L. *J. Chem. Ed.* **2005**, *82*(5), 704.

[44] Kleiner-Shuhler, L.; Brittain, R.; Johnston, M.R.; Hipps, K.W. *J. Phys. Chem. C* **2008**, *112*, 14907-14912.

[45] Katz, H.E.; Lovinger, A.J.; Johnson, J.; Kloc, C.; Siegrist, T.; Li, W.; Lin, Y.Y.; Dodabalapur, A. *Nature* **2000**, 404, 478-481.

[46] Mukhopadhyay, P.; Iwashita, Y.; Shirakawa, M.; Kawano, S.; Fujita, N.; Shinkai, S. *Angew. Chem. In. Ed.* **2006**, *45*, 1592-1595.

[47] Bhosale, S.V.; Jani, C.H.; Langford, S.J. *Chem. Soc. Rev.* **2008**, *37*, 331-342.

[48] Bai, C. *Scanning Tunneling Microscopy and Its Applications 2nd Ed.* **1992**, Springer-Verlag, Berlin, Heidelberg, NewYork.

[49] Biegelsen, D.K.; Ponce, F.A.; Tramontana, J.C. *Appl. Phys. Lett.* **1987**, *50*, 696.

[50] ThermoMicroscopes, 1171 Borregas Avenue, Sunnyvale, CA 94089-1304 http://www.thermomicro.com

[51] Hipps, K.W. In *Handbook of Applied Solid State Spectroscopy*; Vij, D.R., Ed.; Springer Verlag: New York, **2006**; 305.

[52] Schirmeisen, A.; Cross, G.; Stalder, A.; Grütter, P.; Dürig *Appl. Surf. Sci*. **2000**, *157*, 274-279.

[53] Hoffrogge, P.; Kopf, H.; Reichelt, R. *J. Appl. Phys.* **2001**, *90*, 5322.

[54] Naitoh, Y.; Takayanagi, K.; Tomitori, M. *Surf. Sci.* **1996**, *357-358*, 208-212.

[55] Greiner, M.; Kruse, P. *Review of Scientific Instruments*, **2007**, *78*, 026104.

[56] Lucier, A.S. *M. Sc. Thesis*, McGill University, Montreal, Canada, **2004**.

[57] Melmed, A.J. *J. Vac. Sci. Technol. B* **1991**, *9*, 601.

[58] Wiederrecht, G.; Svec, W.; Niemczyk, M.; Wasielewski, M. *J. Phys. Chem.* **1995**, *99*, 8918.

[59] GaussView, Version 3.09, Dennington II, R.; Keith, T.; Millam, J.; Eppinnett, K.; Hovell, W.L.; Gilliland, R.; Semichem, Inc., Shawnee Mission, KS, 2003.

[60] Sugiyama, K.; Yoshimura, D.; Miyamae, T.; Miyazaki, T.; Ishii, H.; Ouchi, Y.; Seki, K. *J. Appl. Phys.* **1998**, *83*, 4928.

[61] Fuller, M.J.; Wasielewski, M.R. *J. Phys. Chem. B* **2001**, *105*, 7216.

[62] Gosztola, D.; Niemczyk, M.P.; Svec, W.; Lukas, A.; Wasielewski, M.R. *J. Phys. Chem. A* **2000**, *104*, 6545.